Optimum Design of a 1x2 Mechanical Optical Switch

Tien-Tung Chung, Chen-Cheng Lee, Kuang-Chao Fan

Department of Mechanical Engineering, National Taiwan University, Taipei 10617, Taiwan, ROC

Abstract This paper studies the optimum design of a 1x2 mechanical optical switch. First, a novel switch configuration is designed with an included anti-thermal mechanism. Then, parametric programs to automatically generate the solid model and to analyze thermal behavior of the switch are developed. From the analysis of the initial design, it revealed that the amount of transverse offset between fiber tips failed in satisfying the Bellcore's specifications. Finally, an integrated program combining CAD software, genetic algorithms, and finite element software was developed for optimum design of optical switches. With the capability of continuously changing critical design parameters of the switch in the integrated design program, the final optimum design satisfying the design constraints and specifications can be found.

Keywords: Optical switch · Structural optimization · Anti-thermal design · Parametric design · Thermal analysis

1 Introduction

In recent years, research on the applications of optical switches has grown rapidly. Chang et al. (2000) developed a mechanical switching apparatus comprised of an output fiber alignment head with a V-groove and a switching member arranged to pivot between first and second positions. The design of this switching mechanism leads to the bending of the input fiber tip when the fiber is pushed against the V-groove. For the switching operation, the apparatus employs many other types of

actuators used in optical switches, such as a thermal actuator developed by Hoffmann et al. (1999) and an electrostatic actuator developed by Spahn et al. (2000).

The optical switches are typically subjected to a range of ambient temperature changes. Due to different thermal expansion coefficients of switch components materials, these temperature changes cause a misalignment of the input fiber tip and the output fiber tip. In response to this kind of thermal misalignment problem, Morey and Glomb (1991) developed a temperature-compensated optical waveguide light filtering device. The fiber is attached to two compensating members made of materials with different thermal expansion coefficients. In this device, the lengths of both the compensating members and the optical fibers will be changed to compensate the misalignment. Yoffe et al. (1995) assembled a passive temperature-compensating package for fiber gratings. The grating is mounted in a package consisting of two materials with different thermal expansion coefficients. A silica tube is used as the low thermal expansion component and an aluminum tube works as the high thermal expansion component. In this design, the aluminum tube was used as the compensating member during ambient temperature changes.

Generally, the electric wire of the actuator serves as the main heat source of the switch. Lau and Buist (1997) calculated the power generation performance of a thermoelectric device for steady-state conditions using the finite element method (FEM). The non-uniform temperature distributions due to the heat source result in the misalignment of the input fiber tip and the output fiber tip. Using the finite difference method (FDM), Leung et al. (1996) determined a thermal modeling procedure to calculate the temperature distribution of components in complex 3D switches and relays. Furthermore, Sircilli et al. (2001) indicated that integrated photonic devices are particularly sensitive to temperature variations. The FEM was

used to perform both thermal and modal analysis of a thermo-optically induced waveguide switch.

Parametric design could prove beneficial in the conservation of cost and time. A variety of general purpose CAD software, such as AutoCAD and Pro/ENGINEER, are capable of parametric design of complex components and systems. Prasead and Somasundaram (1992) devised a Computer-Aided Die Design System (CADDS) for sheet-metal blanks. The system was implemented by incorporating high-level languages Fortran77 and AUTOLISP into AutoCAD for parametric programming. Also, several general purpose FEM programs, such as ANSYS and Nastran, can be used to compute the responses of devices automatically in terms of design parameters. Hieke (1999) demonstrated procedures for the simulation of 3D capacitance in on- and off- chips by utilizing ANSYS-Multiphysics, extended with an APDL (ANSYS Parametric Design Language) macro file. This facilitates the usage of the ANSYS's advanced 3D capabilities to generate, edit and visualize realistic 3D structures.

The structural optimization of the switch depends upon performance, cost and reliability. Genetic algorithm (GA) first developed by Holland (1975) is composed of stochastic search techniques based on the principles of natural genetics and natural selection for global optimization. However, an integrated program that combines both CAD software and FEM software for solving structural optimization problems lacks sufficient development. Wang and Zhao (2002) devised programs that employ the APDL language in ANSYS software to generate an optimal control program that can automatically build, solve, and retrieve results for the model. Schneider et al. (2002) demonstrated another method by partitioning the optimization cycle into model generation, simulation, error calculation and optimization. In an integrated process developed by Botkin (2002), parametric modeling was coupled with

structural optimization to carry out design studies for an automotive body component.

In this paper, a novel switch is first designed utilizing line-to-line and fiber-to-fiber configurations. An anti-thermal mechanism counteracts the axial offset of the fiber tips induced by the ambient temperature changes. Then, a parametric design program is developed to automatically generate the solid model of the switch. The resulting solid model of the switch is exported in ACIS SAT file format and sent to ANSYS finite element software for thermal analysis. In order to automatically analyze the thermal behavior of the switch, the design includes another parametric analysis program using the APDL language. In accordance with Bellcore specifications, three types of loading and boundary conditions are defined and applied to the FEM model for computing the thermal behavior of the switch. ANSYS computes the temperature distributions and thermal deformations of the switch for these three conditions. The analysis of the initial design indicates that the transverse deformation between the input and output fiber tips is too large to satisfy Bellcore specifications. Therefore, an integrated optimum design program, combining the CAD software, FEM software, and GA, is developed and installed for the final optimum design of the switch. With the program's capability of continuously changing the switch's critical design parameters, the goal of the optimization process is to find the global optimum design of the optical switch satisfying the design constraints. It is also required that the transverse deformation between two fiber tips of the optimum design has to comply with Bellcore specifications. The analysis and results of the optimum design prove that the developed integrated optimum design program can be incorporated effectively into analysis and design of the optical switch.

2 Design of mechanical optical switches

The goal of this paper is to design a new 1x2 mechanical optical switch with an anti-thermal mechanism to balance the axial offset of fibers due to ambient temperature changes. The switch should have a novel switching mechanism with low optical loss, low impact on thermal effects, and reliable performance. To improve the alignment discrepancy in the switch design, the input fiber and output fibers are aligned according to the line-to-line configuration. Furthermore, the rotational radius of the switching arm should be shortened.

2.1 The concept design

As shown in Table 1, the design specifications of the switch take the temperature cycling tests and insertion loss tests into account. In the standard temperature cycling tests, the switch should be subjected to an ambient temperature change from -40˚C to 75˚C. In the standard insertion loss tests, to maintain an insertion loss of less than 1 dB in the single mode fiber which its core diameter is 9μm, the axial offset and transverse offset, as shown in Fig. 1, must be controlled to fall within 30μm and 1μm, respectively (see Peter et al. (2002)).

Fig. 2 shows the proposed schematic configuration of the 1x2 mechanical optical switch, and Fig. 3 details the exploded isometric view of the switch. Cross-sectional views of the two switching positions of the switch are shown in Fig. 4a and b, respectively. The switch consists of one input fiber, two output fibers, two fiber holders, two V-grooves, one electric relay, and an anti-thermal mechanism. The electric relay switches the arm between two output fibers into two stable positions. The switching mechanism can alternate one of the output fibers between the input fiber and the neighboring output fiber. The input and output fibers are placed on the

input and output fiber holders, respectively. Additionally, two output fiber tips are placed on two corresponding V-grooves formed therein.

2.2. Anti-thermal mechanism design

In this paper, as shown in Fig. 3, an anti-thermal mechanism with a base and a cover is proposed. When the ambient temperature is changed, non-uniform thermal expansion of internal components will result in the misalignment of the input fiber tip and the output fiber tip. The sizes of the base and the cover can be specifically designed to correct this alignment error.

The material properties of the switch's components are listed in Table 2. In the anti-thermal design, the length differences in internal components are corrected by assigning a low thermal expansion coefficient to the length change of the base. With a thermal expansion coefficient of 1.5×10^{-6} mm/mm-˚C, Invar is an appropriate choice as the best material for the base.

The cross-sectional view of these internal components is depicted in Fig. 5. The gap between the input fiber tip and the output fiber tip L_g is generally set to 0.01 mm, as shown. In computing the changes of component lengths for the anti-thermal design, the following conditions are assumed:

- Temperature distribution in all components is uniform.
- Material of each component is uniform.
- Thermal effect of the glue is disregarded.
- Thermal expansions of two fixed components depend on the expansion of the stronger one.

For a given ambient temperature change ΔT, the total length change of all

internal components ΔL_{os} is expressed in (1), and the length change of the base between the two mounting points A and B ΔL_h shown in Fig. 5 is stated in (2). To balance the length changes of the switch, two changes in length, ΔL_{os} and ΔL_h, must be equal, and component lengths of the switch must satisfy (3) and (4).

$$\Delta L_{os} = (\alpha_s L_{ih} + \alpha_{sm} L_{if} + \alpha_{sm} L_{of1} + \alpha_L L_v + \alpha_{sm} L_{of2})\Delta T \quad (1)$$

$$\Delta L_h = \alpha_I L_b \Delta T \quad (2)$$

$$\alpha_s L_{ih} + \alpha_{sm} L_{if} + \alpha_{sm} L_{of1} + \alpha_L L_v + \alpha_{sm} L_{of2} = \alpha_I L_b \quad (3)$$

$$L_{ih} + L_{if} + L_g + L_{of1} + L_v + L_{of2} = L_b \quad (4)$$

where ΔL_{os} is the total length change of internal components, α_s is the thermal expansion coefficient of Silica, L_{ih} is the glue length of input fiber holder, α_{sm} is the thermal expansion coefficient of the Single Mode Fiber 28 (SMF 28) fiber, L_{if} is the input fiber length between input fiber holder and gap, L_{of1} is the length of output fiber in the V-groove without glue, α_L is the thermal expansion coefficient of the Liquid Crystal Plastics (LCP) V-groove, L_v is the glue length of output fiber in the V-groove, L_{of2} is the length of output fiber between the V-groove and the output fiber holder, ΔT is the ambient temperature change, ΔL_h is the length change of the inner base, α_I is the thermal expansion coefficient of Invar, and L_b is the inner base length. Based on the thermal balance equations (1)-(4), a set of component sizes are provided for the switch, and the proposed final design is shown in Fig. 3.

3 Thermal analysis of mechanical optical switches

The switch design described in this paper is required to pass the temperature cycling

tests in accordance with Bellcore specifications. Due to varying material thermal expansion coefficients, different thermal deformations in the internal components of the switch result in the misalignment of the input fiber tip and the output fiber tip. The thermal behaviors of the switch must be known in advance to correct the misalignment. Additionally, this paper investigates the temperature distributions and thermal deformations of the whole switch structure as well as its components.

3.1 Internal heat generation of the switch

The thermal behaviors of this optical switch are explained in terms of mass, thermal properties, internal heat generation, conduction heat flow, and convection heat flow of the analyzed problem. Radiation heat flow of the switch is negligible and thus disregarded in the thermal analysis.

The electric wire in the actuator serves as the main heat source of the switch. As shown in Fig. 6, the bottom surface of the switching plate, to which the electric wire is adhered, is assumed to be the only heat source in the thermal analysis. Furthermore, the heat generation is presumed to be uniformly distributed over this surface. Fig. 7 demonstrates that an alternating current (AC) voltage with amplitude V_n and frequency ω is used to drive the actuator. The heat generation rate of the electric wire per unit area $\dot{Q}$ can be evaluated by the following equation.

$$V(t) = V_n \sin(\omega t) \tag{5}$$

$$Q(t) = I(t)V(t) = \frac{V^2(t)}{R} = \frac{V_n^{\,2} \sin^2(\omega t)}{R} \tag{6}$$

$$\dot{Q} = \frac{(\int_0^{\pi/\omega} Q(t)dt)/(\frac{\pi}{\omega})}{A} = \frac{\frac{\omega}{\pi}\int_0^{\pi/\omega} V_n^{\,2} \sin^2(\omega t)dt}{RA} = \frac{V_n^{\,2}}{2RA} \tag{7}$$

where $V(t)$ is the voltage at time t, V_n is the voltage amplitude, ω is the

frequency, $Q(t)$ is the heat generation at time t of the electric wire, $I(t)$ is the current at time t, and R is the coil resistance, $\dot{Q}$ is the heat generation rate of the electric wire per unit area, and A is the area of heat source.

Estimating the convective heat transfer coefficients of the air flow in the switch is a prerequisite for thermal analysis of the switch. The air flow in the square cross-sectional switch is assumed to be laminar, thermally fully developed, and with uniform heat flux. In this situation, the Nusselt number Nu for heat transfer is generally described as Nu =3.614 (see Bejan (1993)). Therefore, the convective heat transfer coefficients of the air flow in the switch h are estimated by the following equation.

$$h = \frac{Nu \cdot k}{D_h} \tag{8}$$

where h is the convective heat transfer coefficient of air flow, Nu is the Nusselt number, k is the thermal conductivity of air, and D_h is the hydraulic diameter. As shown in Fig. 3, for the current design, D_h can be calculated as (see Fox and McDonald (1998)):

$$D_h = \frac{4A_c}{P} = \frac{4 \cdot (28 \cdot 32)}{2 \cdot (28 + 32)} = 30 \ \text{(mm)} \tag{9}$$

where A_c is the cross-section area (mm^2), P is the perimeter (mm).

The heat transfer coefficients of the air flow in the switch for temperatures at -40˚C, 25˚C and 75˚C have been computed and listed in Table 3. The electrical and thermal properties of the actuator are also recorded in Table 3.

3.2 Finite element model

The solid model of the switch was originally generated in AutoCAD from given design parameters. The model was exported to an ACIS SAT file by AutoCAD, and

then imported to ANSYS to establish the FEM meshes for the switch. The number of nodal points and the degrees of freedom needed for the switch depend on the complexity of the design and the analysis's required level of the precision. In ANSYS, solid element type SOLID 70 is used for the temperature distribution analysis, and SOLID 45 aids in performing the thermal deformation analysis. In the analysis model, three cases of thermal boundary conditions are applied:

- Case 1: ambient temperature is 25˚C
- Case 2: ambient temperature cycles from 25˚C to 75˚C
- Case 3: ambient temperature cycles from 25˚C to -40˚C

After applying these boundary conditions and heat generation thermal loadings to the FEM model, the steady-state non-uniform temperature distributions can be computed by ANSYS. After obtaining the non-uniform temperature distributions of the switch structure, ANSYS can determine the thermal deformation of the switch with structural boundary conditions set forth in Fig. 6.

3.3 Thermal analysis results of the initial design

For the thermal boundary condition in case 1, Fig. 8a illustrates the temperature distribution, and Fig. 8b displays thermal deformation. Fig. 8a demonstrates that the high temperature region occurs in the relay. According to Fig. 8b, large thermal deformation occurs in the relay and two V-grooves. For boundary conditions of case 2 and case 3, thermal deformations of the switch are shown in Fig. 9a and b, respectively. In these two figures, large thermal deformations also occur in the relay and two V-grooves. The two figures indicate that large thermal deformations occur in the relay and two V-grooves and that case 2 and case 3 have different misalignment types. For case 2, the output fiber tips are bounced up, and in case 3, the output fiber

tips are bumped downward. Table 4 summarizes the results of the thermal analysis of the initial design. In general, a high non-uniform temperature distribution leads to large thermal deformations and causes misalignment of the input fiber tip and the output fiber tip of the switch.

4 Optimum design of mechanical optical switches

With the included anti-thermal mechanism, the analyzed axial offsets of fiber tips in all cases of the initial design are much less 30μm and thus satisfy the insertion loss tests of Bellcore specifications. But, the analyzed transverse offsets of fiber tips in cases 2 and 3 of the initial design are not less than the 1.0μm needed to satisfy the insertion loss tests of Bellcore specifications. Thus, redesign of the optical switch is required to improve the transverse offsets of fiber tips. In this paper, the optimization problem is formulated by selecting five critical design variables and considering the transverse offset of fiber tips as the objective function. An integrated optimum design program combining 3-D CAD software, AutoCAD 2002, finite element software, ANSYS 7.0, and genetic algorithm package, GAlib (see Wall (1996)) is properly suited for optimum design of optical switches.

4.1 Structural optimization problem

The numerical optimization problem can be written in the following form:

$$\begin{aligned} &\text{Find } \vec{x}, \\ &\text{such that } F(\vec{x}) \to \min. \\ &\text{subject to } g_i(\vec{x}) \le 0, i = 1,2,...,n_c \end{aligned} \tag{10}$$

where $\vec{x}$ is the design vector, $F(\vec{x})$ is the objective function, $g_i(\vec{x})$ is the *i-th* constraint, and n_C is the number of constraints.

As shown in Fig. 10, the optimization problem of the optical switch is formulated by selecting five geometric parameters $(X_i,\ i=1,2,...,5)$ of the switch as the design variables. Besides, as shown in Fig. 11, the transverse offsets of fiber tips in thermal boundary condition case 2 $d_{75}(\vec{x})$ and in thermal boundary condition case 3 $d_{-40}(\vec{x})$ are selected as the multi-objective function. The optimization problem is formulated as:

Find $\vec{x}$,

such that

$$F(\vec{x}) = C_1 d_{75}(\vec{x}) + C_2 d_{-40}(\vec{x}) \to \min.$$

subject to

$$\begin{aligned} &0.5\ \text{mm} < X_1 < 3\ \text{mm} \\ &0.1\ \text{mm} < X_2 < 0.2\ \text{mm} \\ &0.5\ \text{mm} < X_3 < 1.5\ \text{mm} \\ &0.4\ \text{mm} < X_4 < 0.6\ \text{mm} \\ &2\ \text{mm} < X_5 < 4\ \text{mm} \end{aligned} \tag{11}$$

where C_1 and C_2 are the weighting coefficients of the objective functions $d_{75}(\vec{x})$ and $d_{-40}(\vec{x})$. As stated in section 2.1, the transverse offset of fiber tips must be less than 1.0μm to satisfy the insertion loss tests of Bellcore specifications. For the initial design, $\vec{x}_0$=(1, 0.171, 1, 0.5,3) , $d_{75}(\vec{x}_0)$=1.75μm, and $d_{-40}(\vec{x}_0)$=1.24μm. Therefore, C_1 is assigned a larger value than C_2. Thus, C_1 and C_2 can be solved by:

$$C_1 + C_2 = 1.0 \tag{12}$$

$$\frac{C_1}{C_2} = \frac{1.75-1}{1.24-1} \tag{13}$$

The solution of the above two equations is C_1=0.76 and C_2=0.24.

4.2 Integrated optimum design program

This integrated optimum design program requires four modules: model generation, FEM simulation, optimization, and execution control. The configuration of the

integrated optimum design program is shown in Fig. 12.

- Model generation

The model in need of optimization contains many adjustable geometrical parameters. Since the sizes of the geometrical configuration parameters in the model must be changed continuously throughout the design process, a parametric design program must be developed to automatically generate the 3D model within general purpose 3D CAD software, such as AutoCAD. AutoCAD is a popular 3D CAD software program that provides both LISP (AutoLISP) and Microsoft Visual C++ (ObjectARX) user interfaces for user customization of the design process. The integrated optimum design program has a parametric-based 3D modeling program within AutoCAD. In the design procedure, geometric parameters of the model are defined first; then, the 3D model is generated by the parametric-based 3D modeling program. Finally, the resulting 3D model is exported to an ACIS SAT or IGES file. Whenever the parameters are changed, the revised 3D model can be generated easily with the parametric-based program.

- FEM Simulation

Since the parametric 3D models are imported into finite element software, a parametric simulation program is necessary to automatically analyze the 3D model. ANSYS is a popular finite element software program featuring macro programs that use APDL, a scripting language that is used to automate meshing and analysis the model in terms of parameters (variables). In the simulation procedure, the 3D model is first imported to the ANSYS software for establishing the meshes of the switch. After applying boundary conditions and loadings to the meshes, thermal and structural responses can be computed. The integrated program has a parametric-based analysis program within ANSYS. Therefore, whenever the model is modified, the revised 3D model can be reanalyzed easily with the developed

parametric-based program.

- Optimization

The optimum design deals with the problem of minimizing or maximizing an objective function in the presence of equality and/or inequality constraints. As for the optimization methods that can be adopted for this study, both the GA and gradient-based methods can be used. The gradient-based optimization methods are efficient, but are usually regarded as local optimization methods. The GA are considered as a global optimization methods, but they need more functional evaluations to find the global optimum design. From a preliminary study of this problem, it is found that there are some local optimum designs in the design space. So, GA is chosen as the optimization method for this problem. Genetic algoritm solves the optimization problem of the optical switch by selecting the best parameters for designing switches with enhanced performances. In the GA, the initial population is generated randomly. The individuals in the resulting population should satisfy all constraints. The fitness of each individual in the population is evaluated. Based on their fitness, Roulette Wheel Selection determines the parents for crossover and mutation operations. Crossover and mutation operations with given probabilities are applied, and two offspring are generated. Through these processes, better individuals gain increased chances of surviving in the next generation. After evolving for several generations, the GA will converge to the optimum solution.

4.3 The optimum optical switch design

The GA parameters used in optimum design of the optical switch are listed in Table 5. Since the population size should be increased with the problem size, a simple

procedure for calculating the population size is $N = 10 \cdot n$, where n is the number of design variables in an optimization problem. Therefore, the population size in this problem is 50. The GA process is considered converged when 95% individuals of the population share the same fitness value. For this problem, about 50 generations are required for obtaining converged solutions.

The best objective function in each generation is shown in Fig. 13. According to the figure, the GA converges within 50 generations. The comparison of the initial and optimum design, recorded in Table 6, shows that the transverse offset of fiber tips is 0.771μm for thermal boundary conditions in case 2 and 0.567μm for case 3. So, the transverse offsets of fiber tips in the optimum design are less than 1.0μm, and thus satisfy the insertion loss tests of Bellcore specifications. The comparison of the geometries between the original design and the optimum design are shown in Fig. 14. Comparison of the thermal deformation between the original design and the optimum design are shown in Fig. 15 and 16. According to Fig. 15 and 16, larger thermal deformation occurs in the relay and two V-grooves in both the initial and optimum designs of case 2 and case 3. In addition, the deformation distributions of the key switch components such as the relay and two V-grooves in the optimum design are smaller than those in the initial design. Therefore, the misalignment of two fiber tips can be reduced by the optimization process in case 2 and case 3. Case 2 and case 3 have different misalignment types. For case 2, the output fiber tips bend up in both the initial and optimum designs. However, in case 3 the output fiber tips bend down in both the initial and optimum designs.

5 Conclusions

This paper studies the optimum design of a 1x2 mechanical optical switch. First, the

mechanical optical switch is designed with line-to-line and fiber-to-fiber configurations. An anti-thermal mechanism is included to compensate for the axial offset of fiber tips due to ambient temperature changes. Then, the temperature distributions and thermal deformations of the switch are computed by ANSYS finite element software. The analysis results show that high non-uniform temperature distributions will cause large thermal deformations. The results also indicate that the transverse offsets of fiber tips in case 2 and case 3 of the initial design are not less than 1.0μm to satisfy the insertion loss tests of Bellcore specifications. Finally, an integrated optimum design program is developed for analysis and optimum design of mechanical optical switches. This program combines a parametric design program written in AutoLISP language, a parametric analysis program written in ANSYS APDL language, and a GAlib genetic algorithm package written in Microsoft Visual C++ language. By using the integrated program, the cycle time for the optimum design process of the optical switch can be shortened.

A final optimum design of the optical switch is obtained from the design result of the integrated program. For the optimum design, the transverse offset between two fiber tips is 0.771μm when the ambient temperature changes from 25˚C to 75˚C (case 2), comparing to the value of 1.747μm for the initial design. When the ambient temperature changes from 25˚C to -40˚C (case 3), the transverse offset is 0.567μm for the optimum design, comparing to the value of 1.238μm for the initial design. It has 56% and 54% improvements on transverse offset between two fiber tips for case 2 and case 3, respectively.

Acknowledgment The optimization program for this paper used the GAlib genetic algorithm package, written by Mattew Wall at the Massachusetts Institute of Technology (http://lancet.mit.edu/ga/).

References

Bejan, A., (1993) **Heat transfer**. John Wiley & Sons Inc, Canada.

Botkin, M.E., (2002) Structural optimization of automotive body components based on parametric solid modeling. Engineering with Computers 18: 109-115.

Chang, C.L., Yeh, C.Y., Smith, M.K., Smith, K.M., Rosette, R.A., Straede, R., (2000) Fiber optic switching apparatus and method. US Patent 6,044,186.

Fox, R. W., McDonald, A. T., (1998) **Introduction to fluid mechanics**. John Wiley & Sons Inc, USA.

Hieke, A., (1999) Precise chip and package 3D capacitance simulations of realistic interconnects using a general purpose FEM-tool**.** Electrical Performance of Electronic Packaging (held in San Diego CA, USA). pp 111-114.

Hoffmann, M., Kopka, P., Voges, E., (1999) All-silicon bistable micromechanical fiber switch based on advanced bulk micromachining. Selected Topics in Quantum Electronics 5: 46-51.

Holland, J.H., (1975) **Adaptation in Natural and Artificial Systems**. MIT Press, USA.

Lau, P.G., Buist, R.J., (1997) Calculation of thermoelectric power generation performance using finite element analysis**.** Thermoelectrics (held in Dresden, Germany), pp 563-566.

Leung, C.H., Lee, A., Wang, B.J., (1996) Thermal modeling of electrical contacts in switches and relays. IEEE Transactions on Components, Packaging, and Manufacturing Technology Part A 19: 346-352.

Morey, W.W., Glomb, W.L., (1991) Incorporated Bragg filter temperature compensated optical waveguide device. US Patent 5,042,898.

Peter, Y.A., Herzing, H.P., Dandliker, R., (2002) Microoptical fiber switch for a large number of interconnects: optical design considerations and experimental realizations using microlens arrays. IEEE Journal on Selected Topics in Quantum Electronics 8: 46-57.

Prasad, Y.K.D.V., Somasundaram, S., (1992) CADDS: an automated die design system for sheet-metal blanking. Computing & Control Engineering Journal 3: 185-191.

Schneider, P., Schneider, A., Schwarz, P., (2002) A modular approach for simulation-based optimization of MEMS. Microelectronics Journal 33: 29-38.

Sircilli, F., Franco, M.A.R., Passaro, A., Abe, N.M., (2001) Finite element analysis of thermo-optic integrated photonic devices. Microwave and Optoelectronics Conference 1: 329-332.

Spahn, O.B., Sullivan, C., Burkhart, J., Tigges, C., Garcia, E., (2000) GaAs-based microelectromechanical waveguide switch. Optical MEMS (held in Kauai Hawaii, USA), pp 41-42.

Wall, M., (1996) **GAlib: a C++ library of genetic algorithm components**. Massachusetts Institute of Technology, USA.

Wang, S., Zhao, J., (2002) FEM optimization for robot structure. Industrial Technology 1: 510-513.

Yoffe, G.W., Krug, P.A., Ouellette, F., Thorncarft, D.A., (1995) Passive temperature -compensating package for optical fiber gratings. Applied Optics 34: 6859-6861.

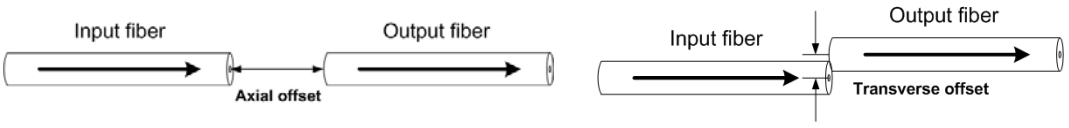

(a) Axial offset (b) Transverse offset

Fig.1 Misalignments between the input fiber tip and the output fiber tip

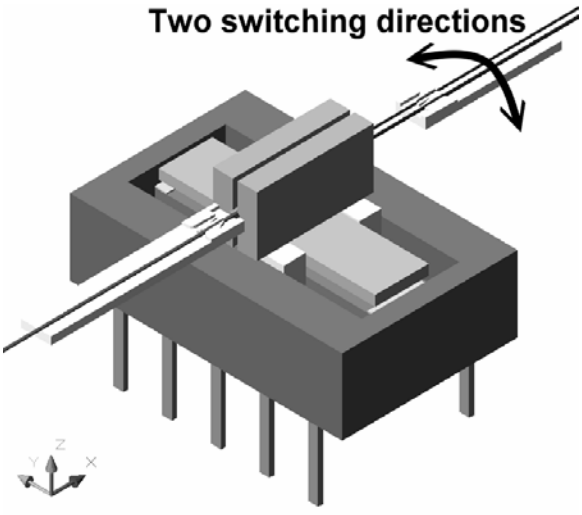

Fig. 2 The switching mechanism of the 1x2 mechanical optical switch

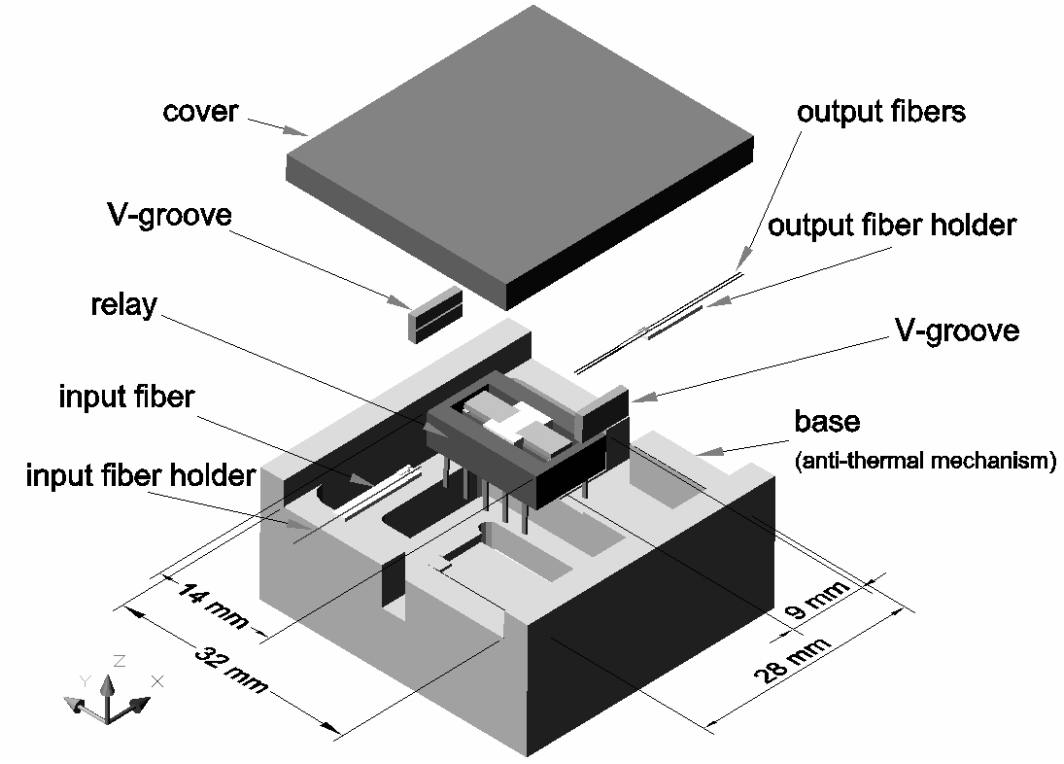

Fig. 3 The exploded isometric view of the 1x2 mechanical optical switch

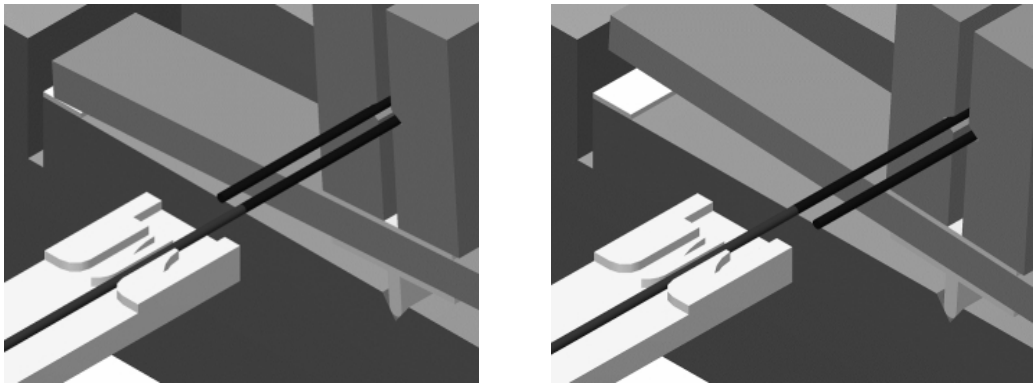

(a) In the right position (b) In the left position

Fig. 4 Cross sectional view of the two switching positions of the optical switch

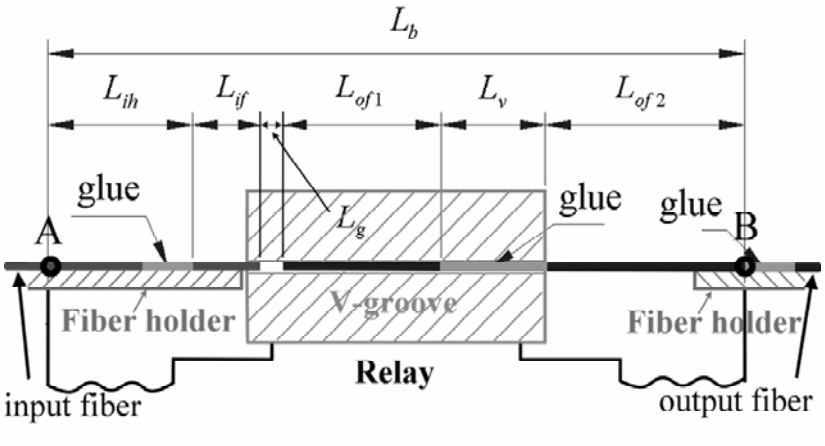

Fig. 5 Cross-sectional view of internal components in the optical switch

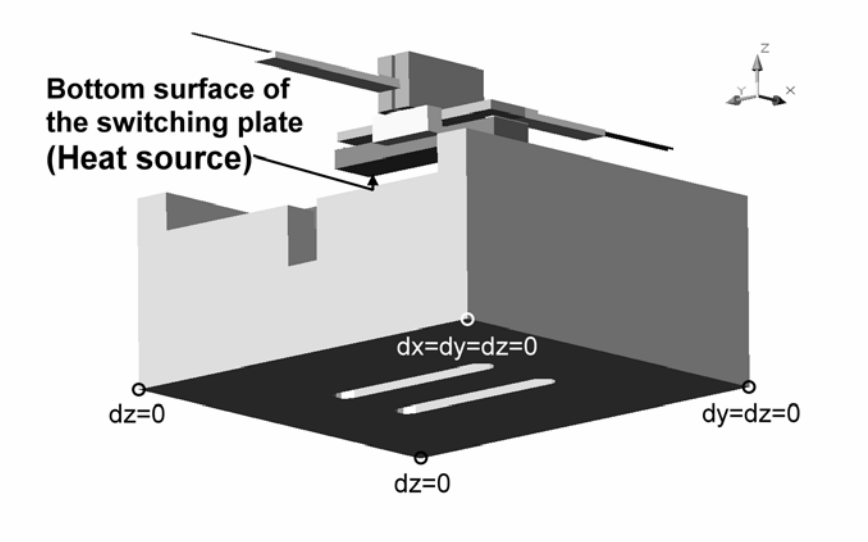

Fig. 6 Heat source and structural boundary conditions of the optical switch

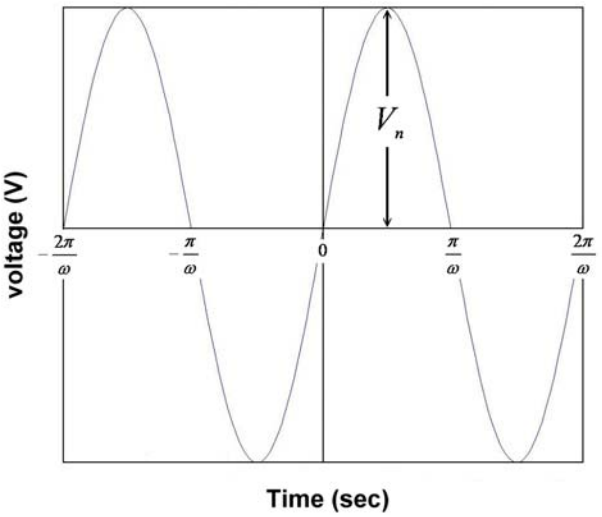

Fig. 7 Alternating current voltage with amplitude V_n and frequency ω

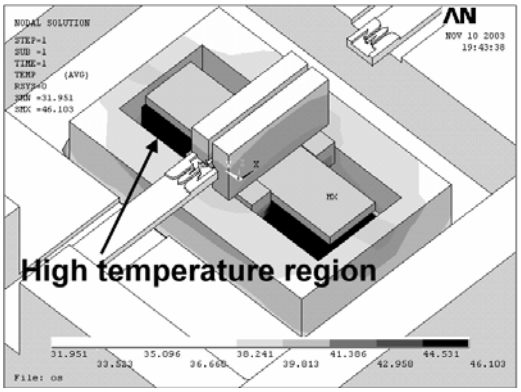

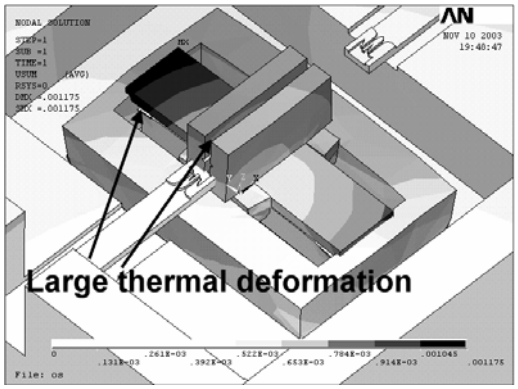

(a) Temperature distribution (˚C) (b) Thermal deformation (mm)

Fig. 8 Case 1: ambient temperature is 25˚C

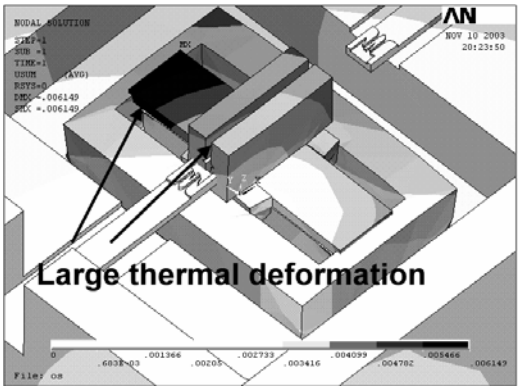

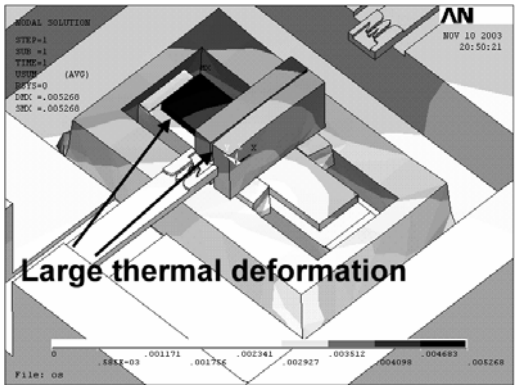

(a) Case 2: ambient temperature cycles from 25˚C to 75˚C

(b) Case 3: ambient temperature cycles from 25˚C to -40˚C

Fig. 9 Thermal deformations (mm) of the switch in case 2 and case 3

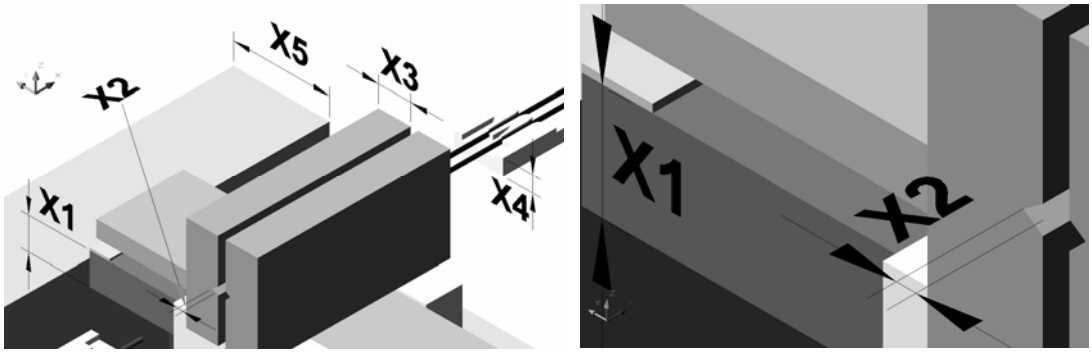

Fig. 10 Design variables of the switch

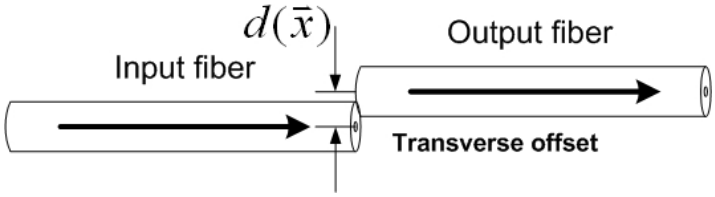

Fig.11 Objective function of the switch

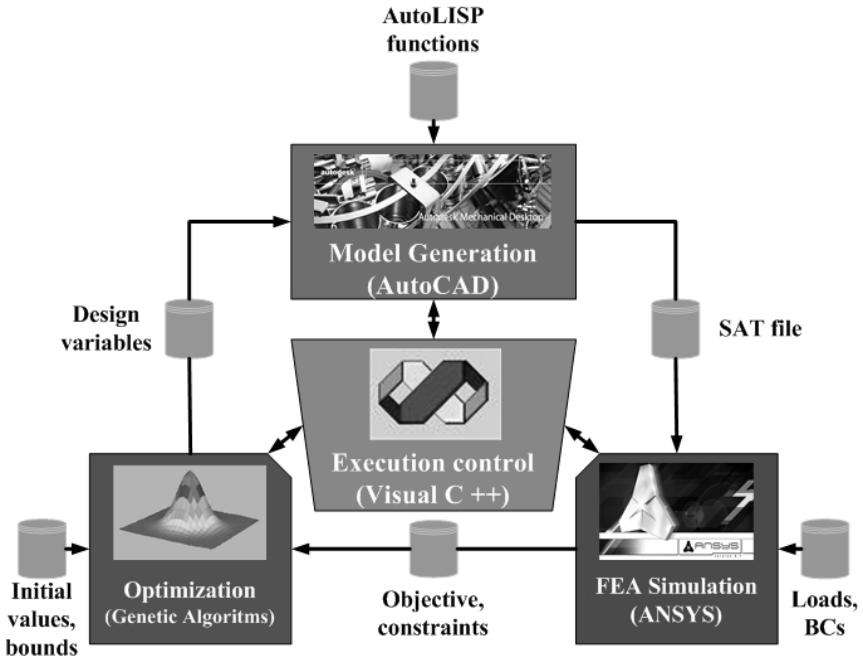

Fig. 12 Configuration of the integrated optimum design program

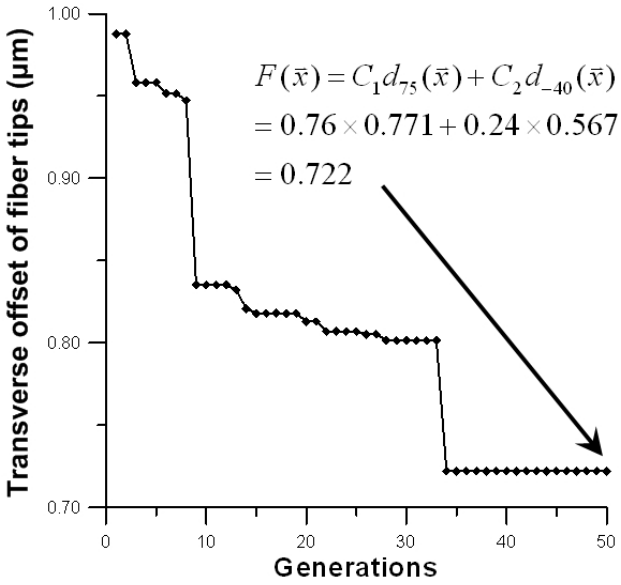

Fig. 13 The best objective function in each generation

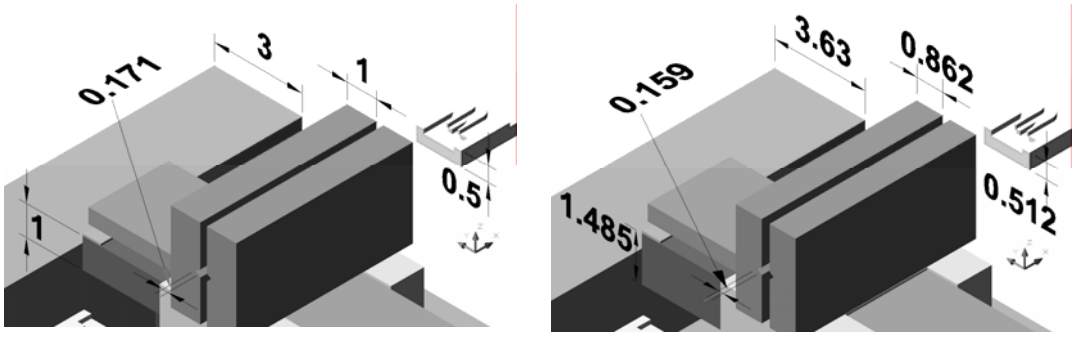

(a) Initial design (b) Optimum design

Fig. 14 Comparison of the switch geometry (mm)

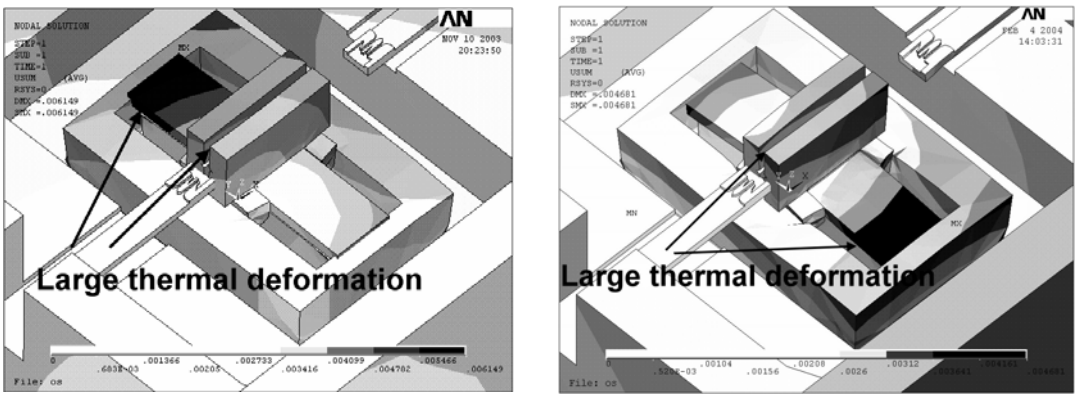

(a) Initial design (b) Optimum design

Fig. 15 Comparison of the switch thermal deformation (mm) in case 2

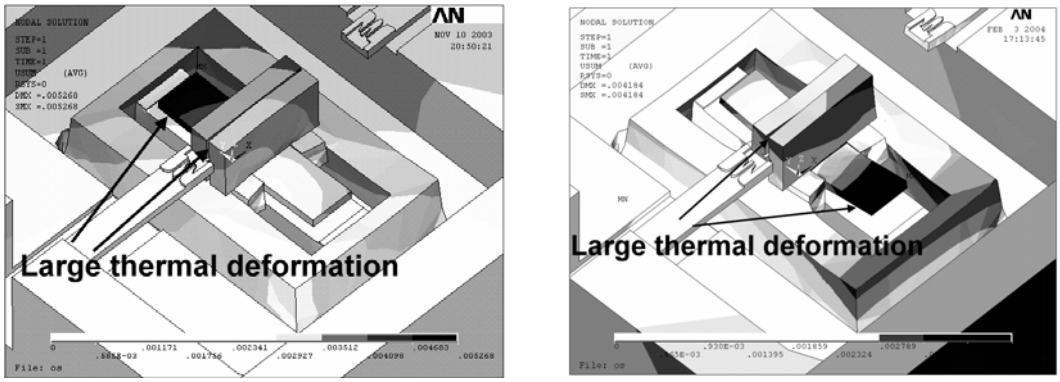

(a) Initial design (b) Optimum design

Fig. 16 Comparison of the switch thermal deformation (mm) in case 3

Table 1 The Bellcore specifications for the optical switch

Temperature cycling tests	Ambient temperature change from -40˚C to 75˚C
Insertion loss tests	Insertion loss should be less than 1 dB

Table 2 Material properties of switch components

	Young's modulus (kgf/mm^2)	Poisson ratio	Thermal conductivity (W/mm-˚C)	Thermal expansion coefficient (mm/mm-˚C)
Silica	7749	0.17	1.4 E-3	0.8 E-6
Invar	14388	0.3	10 E-3	1.5 E-6
LCP*	700	0.33	0.15 E-3	5 E-6
Steel alloy	21122	0.3	51.9 E-3	11.7E-6

*LCP: Liquid Crystal Plastics

Table 3 The electrical and thermal properties of the actuator

Voltage amplitude (V)		5
Coil resistance (ohm)		125
Area of heat source (mm^2)		31.22
Heat generation rate of the electric wire per unit area (W/mm^2)		3.2 E-3
Hydraulic diameter (mm)		30
Thermal conductivity of air (W/mm-˚C)	T= -40˚C	2.08 E-5
	T = 25˚C	2.55 E-5
	T = 75˚C	3 E-5
Convective heat transfer coefficient of air flow (W/mm^2-˚C)	T = -40˚C	2.51 E-6
	T = 25˚C	3.07 E-6
	T = 75˚C	3.61 E-6

Table 4 Thermal analysis results of the optical switch

	Case 1: ambient temperature is 25˚C	Case 2: ambient temperature cycles from 25˚C to 75˚C	Case 3: ambient temperature cycles from 25˚C to -40˚C
Maximum temperature (˚C)	46.103	94.668	-16.748
Maximum thermal deformation (μm)	1.175	6.149	5.268
Axial offset (μm)	0.104	0.448	0.339
Transverse offset (μm)	0.446	1.747	1.238

Table 5 The GA parameters used in optimum design

Population size	50
Generations	50
Crossover rate	0.85
Mutation rate	0.05

Table 6 Comparison of the initial and optimum design

Boundary conditions		Initial design	Optimum design
X_1 (mm)		1.000	1.485
X_2 (mm)		0.171	0.159
X_3 (mm)		1.000	0.862
X_4 (mm)		0.500	0.512
X_5 (mm)		3.00	3.63
Case 1	Axial offset (μm)	0.104	0.097
	Transverse offset (μm)	0.446	0.186
Case 2	Axial offset (μm)	0.448	0.451
	Transverse offset (μm)	1.747	0.771
Case 3	Axial offset (μm)	0.339	0.341
	Transverse offset (μm)	1.238	0.567

Nomenclature

A	Area of heat source (mm^2)
A_c	Cross-section area (mm^2)
P	Perimeter (mm)
C_1	Weighting coefficient of objective functions $d_{75}(\vec{x})$
C_2	Weighting coefficient of objective functions $d_{-40}(\vec{x})$
$d(\vec{x})$	Objective function of optical switch optimization problem (μm)
$d_{75}(\vec{x})$	Transverse offsets of fiber tips in thermal boundary condition case 2 (μm)
$d_{75}(\vec{x}_0)$	Transverse offsets of fiber tips for initial design in thermal boundary condition case 2 (μm)
$d_{-40}(\vec{x})$	Transverse offsets of fiber tips in thermal boundary condition case 3 (μm)
$d_{-40}(\vec{x}_0)$	Transverse offsets of fiber tips for initial design in thermal boundary condition case 3 (μm)
D_h	Hydraulic diameter (mm)
$F(\vec{x})$	Objective function
$g_i(\vec{x})$	*i-th* constraint
h	Convective heat transfer coefficient of air flow (W/mm^2-˚C)
$I(t)$	Current at time t
k	Thermal conductivity of air (W/mm-˚C)
L_b	Inner base length (mm)
L_g	Gap between input fiber tip and output fiber tip (mm)
L_{if}	Input fiber length between input fiber holder and gap (mm)
L_{ih}	Glue length of input fiber holder (mm)
L_{of1}	Length of output fiber in V-groove without glue (mm)

L_{of2}	Length of output fiber between V-groove and output fiber holder (mm)
L_v	Glue length of output fiber in V-groove (mm)
n	Number of design variables in an optimization problem
n_C	Number of constraints
N	Population size
Nu	Nusselt number
$Q(t)$	Heat generation at time t of electric wire (W)
$\dot{Q}$	Heat generation rate of electric wire per unit area (W/mm^2)
R	Coil resistance (ohm)
t	Time
$V(t)$	Voltage at time t (V)
V_n	Voltage amplitude (V)
$\vec{x}$	Design vector
$\vec{x}_0$	Initial design of optical switch optimization problem (μm)
X_i	Design variables of optical switch optimization problem (i=1,2,…,5) (mm)
ΔL_h	Length change of base between two mounting points A and B (mm)
ΔL_{os}	Total length change of all internal components (mm)
ΔT	Ambient temperature change (˚C)
α_I	Thermal expansion coefficient of Invar (mm/mm-˚C)
α_L	Thermal expansion coefficient of LCP V-groove (mm/mm-˚C)
α_s	Thermal expansion coefficient of Silica (mm/mm-˚C)
α_{sm}	Thermal expansion coefficient of SMF 28 fiber (mm/mm-˚C)
ω	Frequency